applied optics

Single-shot absolute 3D shape measurement with Fourier transform profilometry

Beiwen Li, Yatong An, and Song Zhang*

School of Mechanical Engineering, Purdue University, West Lafayette, Indiana 47907, USA
*Corresponding author: szhang15@purdue.edu

Received 11 April 2016; revised 1 June 2016; accepted 2 June 2016; posted 2 June 2016 (Doc. ID 262948); published 27 June 2016

Fourier transform profilometry (FTP) is one of the frequently adopted three-dimensional (3D) shape measurement methods due to its ability to recover single-shot 3D shapes, yet it is challenging to retrieve the absolute phase map solely from one single grayscale fringe image. This paper presents a computational framework that overcomes this limitation of FTP with digital fringe projection (DFP). By using geometric constraints, an absolute phase map can be retrieved point-by-point from one single grayscale fringe image. Experiments demonstrate the success of our proposed framework with single-shot absolute 3D shape measurement capability.

OCIS codes: (120.0120) Instrumentation, measurement, and metrology; (100.5088) Phase unwrapping; (110.5086) Phase unwrapping; (100.5070) Phase retrieval.

http://dx.doi.org/10.1364/AO.55.005219

1. INTRODUCTION

Three-dimensional (3D) shape measurement has become attractive to a variety of applications such as industrial quality control and biomedical imaging. Among existing 3D shape measurement technologies, phase-based approaches have the advantages of high resolution and noise resistance compared to intensity-based approaches. Within phase-based approaches, the well-known phase-shifting profilometry, which uses multiple phase-shifted patterns, is capable of measuring the 3D shape of an object with high quality [1], yet the requirement for projection of multiple patterns may introduce measurement errors when measuring dynamically deformable shapes [2]. Fourier transform profilometry (FTP) [3], which requires only a single fringe projection, has become a quite powerful tool for many applications [4,5] such as vibration measurement of micromechanical devices [6] or instantaneous deformation analysis [7]. However, the retrieval of an absolute phase map within a single fringe image remains a nontrivial problem.

For an accurate 3D shape measurement, the retrieval of an absolute phase map plays an important role in the 3D reconstruction process [8]. Most single-shot FTP frameworks use spatial phase unwrapping in which the obtained phase maps are relative and do not work for spatially isolated objects. Conventional absolute phase recovering methods typically require the projection of additional images such as an additional centerline image projection [9,10], multi-wavelength fringe projection [11–13], or phase coding methods [14,15]. There are also research works that use embedded markers [16] or pattern codifications [17] in different color channels. All these aforementioned frameworks cannot be used to perform FTP fringe analysis within one single-shot 8-bit image. To address this issue, researchers have been attempting to embed marker points [8], marker strips [18–20], or special markers [21] into sinusoidal fringe patterns, and the methods proposed in [18] and [19] incorporated the marker retrieval process with phase shifting, which is not applicable to the single-shot FTP method. Guo and Huang [8] embedded a cross-shape marker into a single sinusoidal pattern and spatially unwrapped the phase from FTP by referring to the phase value of the marker point. Xiao *et al.* [21] embedded a special mark into the sinusoidal grating for a similar purpose. The spectra of the mark are perpendicular to that of the projected fringe and can be retrieved with the bandpass filter in the other direction. Recently, Budianto *et al.* [20] embedded several lines of strip markers within a single fringe pattern and improved the robustness of strip marker detection with dual-tree complex wavelet transformation. However, in general, for all marker-based approaches, a fundamental limitation is that they cannot recover absolute phase for an isolated object if no encoded marker is on the object. Moreover, phase quality could deteriorate on the area covered by the markers.

In this research, we propose a computational framework that performs single-shot absolute phase recovery for the FTP method without any additional marker or color encoding. After phase wrapping from the single-shot FTP method, using the geometric constraints of a digital fringe projection (DFP) system, we create an artificial absolute phase map Φ_{min} and extract the final unwrapped absolute phase map through pixel-by-pixel

reference to Φ_{min}. Experiments demonstrate that our computational framework is capable of reconstructing absolute 3D geometry of both single objects or spatially isolated objects with the single-shot FTP method.

Section 2 introduces the principles of FTP and our proposed framework of absolute phase retrieval. Section 3 presents some experimental validations to demonstrate the success of our proposed method. Section 4 discusses the merits and limitations of the proposed method, and finally Section 5 summarizes this research.

2. PRINCIPLES

This section introduces the relevant principles of this research. In particular, we will explain the theoretical background of FTP, the imaging model of a DFP system, and our proposed absolute phase retrieval framework using geometric constraints.

A. Fourier Transform Profilometry

The basic principle of the FTP method can be illustrated as follows: theoretically, a typical fringe pattern can be described as

$$I(x,y) = I'(x,y) + I''(x,y)\cos[\phi(x,y)], \tag{1}$$

where $I'(x,y)$ represents the average intensity, $I''(x,y)$ denotes the intensity modulation, and $\phi(x,y)$ is the phase to be found. Using Euler's formula, Eq. (1) can be rewritten as

$$I(x,y) = I'(x,y) + \frac{I''(x,y)}{2}[e^{j\phi(x,y)} + e^{-j\phi(x,y)}]. \tag{2}$$

After applying a bandpass filter, which only preserves one of the frequency components, we will have the final fringe expressed as

$$I_f(x,y) = \frac{I''(x,y)}{2}e^{j\phi(x,y)}. \tag{3}$$

In practice, we can use different kinds of windows, such as a smoothed circular window [see Fig. 1(a)] or a Hanning window [22] [see Fig. 1(b)], as bandpass filters. After bandpass filtering, we can calculate the phase by

$$\phi(x,y) = \tan^{-1}\left\{\frac{\mathrm{Im}[I_f(x,y)]}{\mathrm{Re}[I_f(x,y)]}\right\}. \tag{4}$$

Here $\mathrm{Im}[I_f(x,y)]$ and $\mathrm{Re}[I_f(x,y)]$, respectively, represent the imaginary and the real part of the fringe $I_f(x,y)$. With this FTP approach, the wrapped phase with 2π discontinuities can be extracted from a single-shot fringe image.

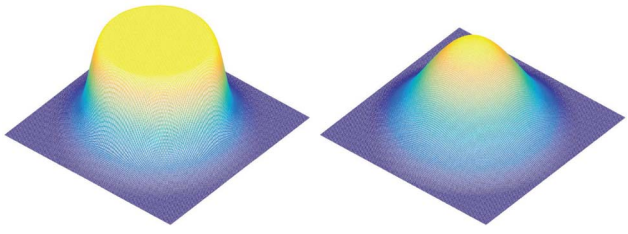

(a) (b)

Fig. 1. Different bandpass filters used for FTP. (a) Smoothed circular window; (b) Hanning window.

Apart from single-shot FTP, there is also a modified FTP method [23] that uses two fringe patterns to retrieve a phase map. One approach for performing double-shot phase retrieval is by using inverted patterns

$$I_1 = I'(x,y) + I''(x,y)\cos[\phi(x,y)], \tag{5}$$

$$I_2 = I'(x,y) - I''(x,y)\cos[\phi(x,y)]. \tag{6}$$

By subtracting the two images, we can obtain

$$I = (I_1 - I_2)/2 = I''(x,y)\cos[\phi(x,y)]. \tag{7}$$

In this way, the effect of a DC component can be significantly suppressed, which helps improve the phase quality, yet also sacrifices the measurement speed by introducing another fringe image.

B. DFP System Model

In this research, we adopt the well-known pinhole model to formulate the imaging lenses of a DFP system. In this model, the projection from 3D world coordinate (x^w, y^w, z^w) to 2D imaging coordinate (u, v) can be formulated as the following equation:

$$s\begin{bmatrix} u \\ v \\ 1 \end{bmatrix} = \begin{bmatrix} f_u & \gamma & u_0 \\ 0 & f_v & v_0 \\ 0 & 0 & 1 \end{bmatrix}\begin{bmatrix} r_{11} & r_{12} & r_{13} & t_1 \\ r_{21} & r_{22} & r_{23} & t_2 \\ r_{31} & r_{32} & r_{33} & t_3 \end{bmatrix}\begin{bmatrix} x^w \\ y^w \\ z^w \\ 1 \end{bmatrix}. \tag{8}$$

Here, s is the scaling factor; f_u and f_v are, respectively, the effective focal lengths of the imaging device along u and v directions; γ is the skew factor of the two axes; r_{ij} and t_i, respectively, represent the rotation and translation parameters; and (u_0, v_0) is the principle point. The model described in Eq. (8) can be further simplified by

$$\mathbf{P} = \begin{bmatrix} f_u & \gamma & u_0 \\ 0 & f_v & v_0 \\ 0 & 0 & 1 \end{bmatrix}\begin{bmatrix} r_{11} & r_{12} & r_{13} & t_1 \\ r_{21} & r_{22} & r_{23} & t_2 \\ r_{31} & r_{32} & r_{33} & t_3 \end{bmatrix}, \tag{9}$$

$$= \begin{bmatrix} p_{11} & p_{12} & p_{13} & p_{14} \\ p_{21} & p_{22} & p_{23} & p_{24} \\ p_{31} & p_{32} & p_{33} & p_{34} \end{bmatrix}, \tag{10}$$

where the projection matrix $\mathbf{P}$ can be estimated using some well-developed camera calibration toolboxes.

In reality, the projector shares the same imaging model with the camera whose optics are mutually inverted. If the camera and projector are calibrated under the same world coordinate system (x^w, y^w, z^w), we can obtain two sets of equations for the DFP system,

$$s^c[\,u^c \quad v^c \quad 1\,]^t = \mathbf{P^c}[\,x^w \quad y^w \quad z^w \quad 1\,]^t, \tag{11}$$

$$s^p[\,u^p \quad v^p \quad 1\,]^t = \mathbf{P^p}[\,x^w \quad y^w \quad z^w \quad 1\,]^t. \tag{12}$$

Here, superscript p indicates the projector; superscript c indicates the camera; and t represents matrix transpose.

In this DFP model, Eqs. (11) and (12) provide six equations with seven unknowns $(s^c, s^p, x^w, y^w, z^w, u^p, v^p)$. To reconstruct the 3D (x^w, y^w, z^w) geometry, we need one more equation, which can be obtained by the linear relationship between absolute phase Φ and a projector pixel line u^p:

$$u^p = \Phi \times T/(2\pi). \tag{13}$$

However, as described in Section 2.A, the phase extracted from FTP is wrapped with 2π discontinuities, and the absolute phase retrieval becomes challenging if we do not refer to any additional fringes or embedded markers. In the next section, we will introduce our proposed framework that retrieves absolute phase within one single fringe without using any embedded markers.

C. Absolute Phase Retrieval Using Geometric Constraints

In theory, if we know the z^w value from prior knowledge, we can then reduce one unknown from the seven unknowns for the six equations in Eqs. (11) and (12); reducing one unknown means that all (u^p, v^p) values can be uniquely determined given (u^c, v^c), and the absolute phase value can be computed by referring to Eq. (13). In other words, for a given $z^w = z_{\min}$, one can create an artificial absolute phase map on the camera image. Furthermore, if $z^w = z_{\min}$ coincides with the closest depth plane of the measured volume, one can retrieve an absolute phase map $\Phi_{\min}$, which is defined here as a minimum phase map:

$$\Phi_{\min}(u^c, v^c) = f(z_{\min}, T, P^c, P^p). \tag{14}$$

As one can see, $\Phi_{\min}$ is a function of $z_{\min}$, the fringe width T, and the projection matrices P^c and P^p. Since this minimum phase map $\Phi_{\min}(u^c, v^c)$ is constructed with the camera pixel, the absolute phase retrieval can be performed by pixel-to-pixel reference to $\Phi_{\min}(u^c, v^c)$.

The key to generating accurate minimum phase map $\Phi_{\min}$ lies in a good estimation of $z_{\min}$. Figure 2 illustrates the schematic diagram of a DFP system. In this research, we match the camera lens coordinate with the world coordinate system. From Fig. 2, one can see that $z_{\min}$ plane has the minimum z^w value from the camera perspective. In practice, one can determine the $z_{\min}$ of interest by a variety of means, one of which being the use of more fringe patterns and measurement of a stationary object (e.g., a plane).

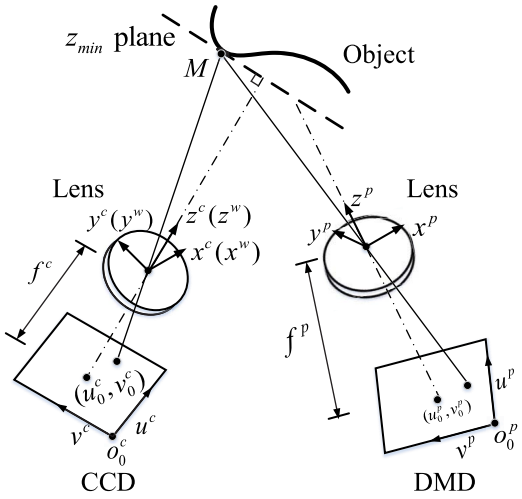

Fig. 2. Schematic diagram of a DFP system and $z_{\min}$ plane; DMD, digital micro-mirror device.

Once we calibrated the DFP system, we obtained all matrix parameters in P^c and P^p. Given $z_{\min}$, we can solve for the corresponding x^w and y^w for each camera pixel (u^c, v^c) by simultaneously solving Eqs. (11) and (12)

$$\begin{bmatrix} x^w \\ y^w \end{bmatrix} = A^{-1} b, \tag{15}$$

where

$$A = \begin{bmatrix} p^c_{31}u^c - p^c_{11} & p^c_{32}u^c - p^c_{12} \\ p^c_{31}v^c - p^c_{21} & p^c_{32}v^c - p^c_{22} \end{bmatrix}, \tag{16}$$

$$b = \begin{bmatrix} p^c_{14} - p^c_{34}u^c - (p^c_{33}u^c - p^c_{13})z_{\min} \\ p^c_{24} - p^c_{34}v^c - (p^c_{33}v^c - p^c_{23})z_{\min} \end{bmatrix}. \tag{17}$$

Here p^c_{ij} denotes the matrix parameters of P^c in the i-th row and the j-th column. Once (x^w, y^w) are determined, we can calculate the corresponding (u^p, v^p) for each camera pixel by solving Eq. (12) again as

$$s^p[\,u^p \quad v^p \quad 1\,]^t = P^p[\,x^w \quad y^w \quad z_{\min} \quad 1\,]^t. \tag{18}$$

Assuming the projected fringe patterns are along the v^p direction, the artificial phase $\Phi_{\min}$ for (u^c, v^c) can be defined as

$$\Phi_{\min}(u^c, v^c) = u^p \times 2\pi/T, \tag{19}$$

where T is the fringe period in pixels used for 3D shape measurement, and the phase is defined as starting at 0 rad when $u^p = 0$.

Figure 3 illustrates the phase-unwrapping scheme using minimum phase $\Phi_{\min}$, in which Fig. 3(a) shows the phase map extracted directly from the FTP method with 2π discontinuities. Figure 3(b) shows the continuous minimum phase map $\Phi_{\min}$ on the projector space. Figure 3(c) shows the cross sections of the phase maps. Assume that the region inside of the dashed red bounding boxes is what the camera captures at $z = z_{\min}$ and that the captured region is shifted to the area inside of the solid blue bounding boxes when $z > z_{\min}$. Under both circumstances, we unwrap the phase map by adding 2π on the wrapped phase map where the phase values are below the corresponding points on $\Phi_{\min}$.

In a more general case where we have more fringe periods in the capture camera image, as shown in Figs. 4(a) and 4(b), we will add different integer K multiples of 2π to remove the

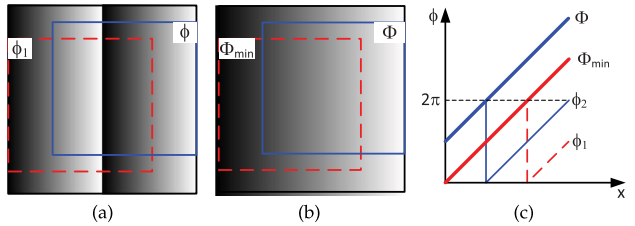

Fig. 3. Concept of removing a 2π jump of a low-frequency phase map by using the minimum phase map determined from geometric constraints. (a) Wrapped phase map ϕ_1 and ϕ captured from the camera; (b) corresponding $\Phi_{\min}$ and Φ defined on the projector; (c) cross sections of $\Phi_{\min}$ and Φ and the phase maps with 2π discontinuities. In parts (a) and (b), windowed regions show phase maps that are acquired by a camera at different depths z: the red dashed windows show $z_{\min}$, and the solid blue windows show $z > z_{\min}$.

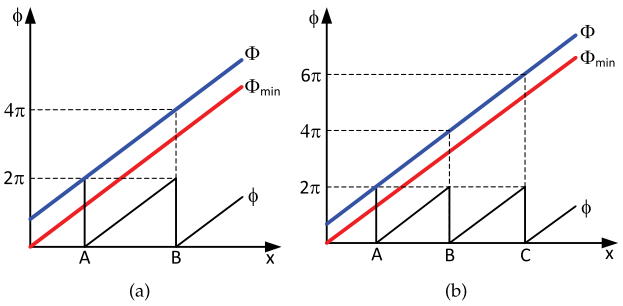

Fig. 4. Determination of the number of 2π or fringe order K for periods of fringe patterns. (a) Three and (b) four periods of fringe patterns.

discontinuities depending on the difference between the wrapped phase ϕ and the minimum phase $\Phi_{\min}$, and the fringe order K is determined by the following equations:

$$2\pi \times (K-1) < \Phi_{\min} - \phi < 2\pi \times K, \tag{20}$$

or

$$K(x,y) = \text{ceil}\left[\frac{\Phi_{\min} - \phi}{2\pi}\right]. \tag{21}$$

Here, ceil[] is the ceiling operator that returns the closest upper integer value. Through this unwrapping framework, we can obtain the absolute phase map Φ without 2π discontinuities without any additional encodings or embedded markers. By using the linear phase constraints in Eq. (13) and the DFP system equations in Eqs. (11) and (12), we can realize absolute 3D shape measurement within a single-shot fringe image through the FTP method.

3. EXPERIMENT

To test the performance of our single-shot absolute 3D shape measurement framework with the FTP method, we developed a DFP system in which a CCD camera (The Imaging Source DMK 23U618) is used as the image capturing device which uses a 2/3-inch imaging lens (Computar M0814-MP2) with a focal length of 8 mm and an aperture of $f/1.4$. A digital light processing (DLP) projector (Dell M115HD) is used as the projection device whose lens has a focal length of 14.95 mm with an aperture of $f/2.0$. Its projection distance ranges from 0.97 to 2.58 m. The resolutions for the camera and the projector are, respectively, 640 × 480 pixels and 1280 × 800 pixels. We calibrated the system using the method discussed in Ref. [24] and chose the world coordinate system to be aligned with the camera lens coordinate system.

We first tested our proposed framework by measuring a sculpture, as shown in Fig. 5(a). Figure 5(b) shows the single-shot fringe image that we captured, and Fig. 5(c) shows the wrapped phase map that we obtained using the FTP method. Figure 5(d) demonstrates the minimum phase map $\Phi_{\min}$ that we generated at the closest depth plane $z_{\min} = 960$ mm of the measurement volume. Figures 5(e) and 5(f) show the unwrapped phase map and the reconstructed 3D geometry, respectively, from the calibrated DFP system, from which we can see that our proposed framework can successfully reconstruct

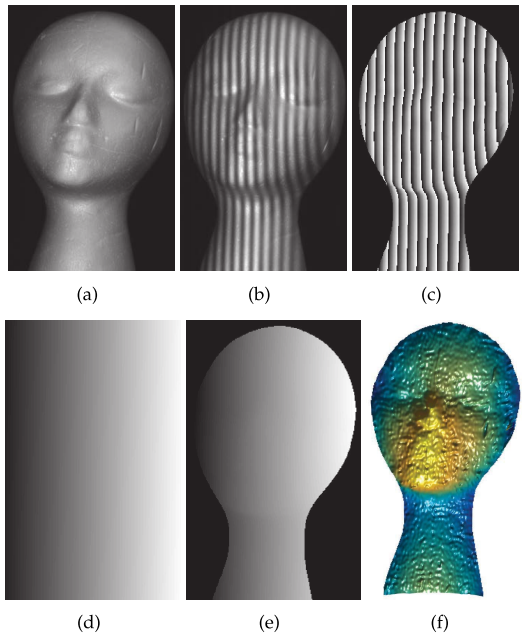

Fig. 5. Illustrations of the unwrapping procedure with a real object measurement. (a) Original picture of the measured object; (b) captured single-shot fringe image; (c) wrapped phase map obtained from single-shot FTP; (d) minimum phase map $\Phi_{\min}$; (e) unwrapped phase map; (f) reconstructed 3D geometry.

the 3D geometry from a single-shot fringe image using FTP. The bandpass filter that we used to suppress unwanted spectral components is a smoothed circular window, as shown in Fig. 1(a). Since we did not involve any additional color or marker encoding, it addresses the phase-unwrapping challenge of conventional single-shot FTP as stated in Section 1.

To verify that our proposed framework indeed produces absolute 3D geometry, we also measured the same object using a standard three-step phase-shifting approach with a binary-coded temporal phase-unwrapping method [25]. The result is shown in Fig. 6(a), which overall agrees well with the 3D result from single-shot FTP with our proposed framework, as shown in Fig. 6(b). Their only difference is that the FTP method has a higher noise level, a fundamental limitation of the FTP method itself that is caused by the remainder of the DC component (see Section 2.A) after the bandpass filter. To suppress the effect of DC component, we also implemented our framework with the modified FTP method [23], as mentioned in Section 2.A. The corresponding 3D result is shown in Fig. 6(c), which demonstrates that our proposed framework also works well with the modified FTP method, and the noise level is significantly reduced. However, these benefits come at the cost of reducing the measurement speed. We then took a cross section around the center of the nose from the three different 3D results and plotted them all in Fig. 7. To better examine their differences, we took the result from the standard phase-shifting approach as the reference and subtracted it from the results obtained from both the FTP and modified FTP methods. The corresponding difference curves for the FTP and modified FTP methods are, respectively, shown in Figs. 8(a) and 8(b), where we can see that the overall 3D

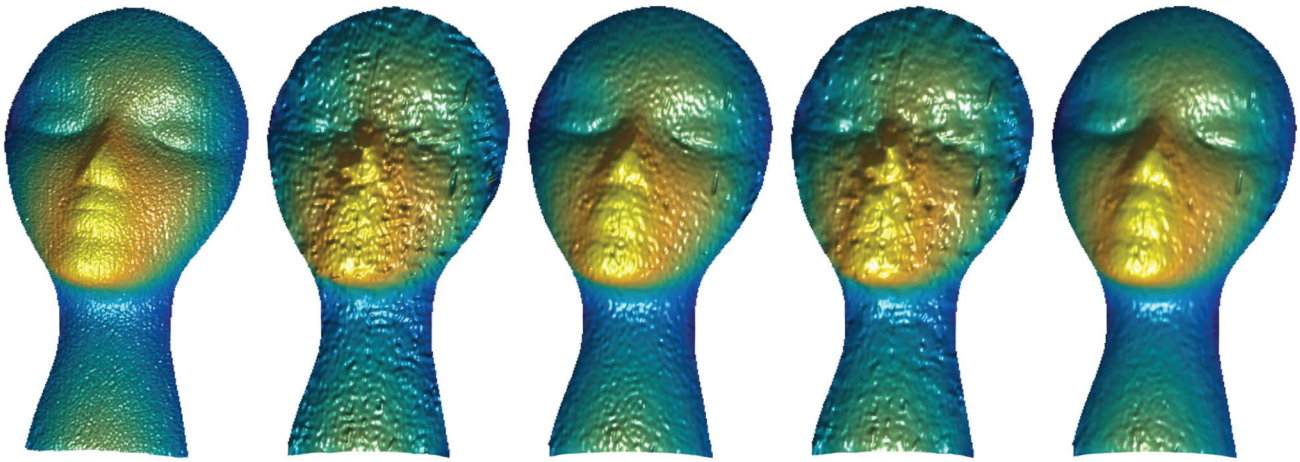

Fig. 6. 3D measurement results of a sculpture. (a) Using standard phase-shifting method plus simple binary coding; (b) using single-shot FTP method with smoothed circular-shaped bandpass filter; (c) using modified FTP method with smoothed circular-shaped bandpass filter; (d) and (e) corresponding results of (b) and (c) using a Hanning-window-shaped bandpass filter.

geometries of both methods indeed match very well with the standard phase shifting with binary coding approach; and the mean difference is almost zero, as expected. Compared with the modified FTP method, the phase obtained from the single-shot fringe pattern has a larger difference because the phase error estimated from a single fringe pattern is larger than that estimated from the modified FTP method, which is anticipated. We also tried a Hanning window [22] as a different bandpass filter [see Fig. 1(b)] for both single-shot and modified FTP methods, and the results are shown in Figs. 6(d) and 6(e), respectively. From these figures, we can see that different bandpass filters will not affect the overall reconstructed geometry of the measured object, but only produce different high frequency noise levels.

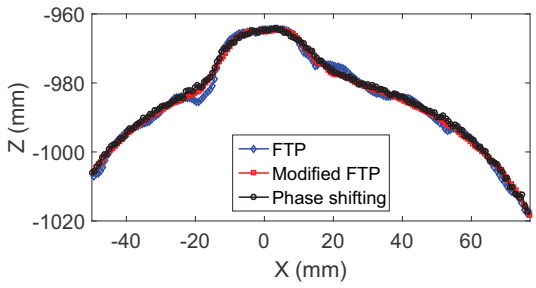

Fig. 7. Cross sections of the 3D results corresponding to Figs. 6(a), 6(b), and 6(c).

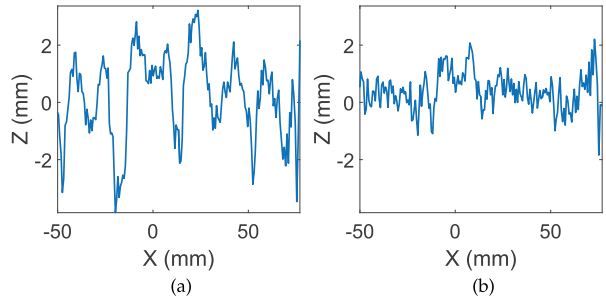

Fig. 8. Difference in geometries between (a) FTP and phase shifting (mean: 0.16 mm, RMS: 1.48 mm) and (b) modified FTP and phase shifting (mean: 0.20 mm, RMS: 0.64 mm).

To demonstrate that our proposed framework, as opposed to a spatial phase-unwrapping framework, also works for spatially isolated objects, we then put a spherical object beside the sculpture and performed 3D shape measurements with all the same methods (i.e., phase-shifting, single-shot FTP, and modified FTP methods) used in the previous experiment. The measurement results are shown in Fig. 9, where Fig. 9(a) shows the captured fringe image, and Figs. 9(b)–9(f) show the reconstructed 3D geometry using the same methods used to produce the 3D results shown in Figs. 6(a)–6(e). From the 3D results, we can see that our proposed framework produces similar measurement qualities as the previous experiment for isolated objects, i.e., the overall profiles obtained from both single-shot and modified FTP methods agree well with the one obtained from the standard three-step phase-shifting method. This experiment confirms that our proposed framework has the capability of measuring the 3D shape of spatially isolate objects within one single-shot fringe image.

4. DISCUSSION

This proposed absolute phase-recovery framework has the following advantages compared to marker-based absolute phase-recovery techniques:

- *Single-shot, absolute pixel-by-pixel 3D recovery.* Using an artificial absolute phase map generated in camera image space, our proposed framework is capable of recovering absolute 3D geometries pixel-by-pixel within one single-shot, 8-bit grayscale fringe image, which is not possible, to the best of our knowledge, with any existing technologies, making it valuable

to absolute 3D shape measurement for extremely high-speed motion capture.

• *Simultaneous multiple objects measurement*. Since phase unwrapping is pixel-by-pixel, as demonstrated in Fig. 9, the proposed method can be used to measure multiple objects at the exact same time, which is extremely difficult to do for conventional Fourier transform methods.

• *Robustness in fringe order determination*. The determination of fringe order K is crucial for absolute phase retrieval, yet the success of marker-based approaches rely on the detection of markers that encode fringe order, which could be problematic when those markers are not clear on a captured fringe image. In contrast, we use an artificially generated absolute phase map $\Phi_{\min}$ for temporal phase unwrapping. Since $\Phi_{\min}$ is ideal and not dependent on the captured fringe quality (besides the inherent camera sensor noise), the robustness of fringe order determination is greatly improved.

• *3D reconstruction of complicated scenes*. As one may notice, the major prerequisite for the success of our proposed approach lies in the assumption that all sampled points of the entire scene should not cause more than 2π phase difference from $z_{\min}$, regardless of the complexity (e.g., number of objects, object isolation, and hidden surfaces) of the measured scenes or the existence of abrupt depth change as long as the corresponding phase jumps are less than 2π.

However, this proposed framework is not trouble free. The major limitations are:

• *Confined measurement depth range*. As mentioned previously, the maximum measurement depth range that our proposed approach can handle is within 2π in phase domain from one pixel to its neighborhood pixels. Therefore, in cases where there are abrupt jumps that introduce 2π phase changes from one pixel to the next pixel, our proposed framework could produce incorrect unwrapped phase. However, the limit of the depth change depends upon the angle between the projector and the camera; the smaller the angle between the projector and the camera, the larger the actual abrupt depth change the proposed method can handle. For instance, in our experiment, we used a fringe period of 18 pixels and an angle of 6° between camera and projector optical axes; the effective depth range is approximately 25% of the lateral sensing range, which results in fairly good measurement depth volume. In the meantime, we are still working on extending the effective sensing

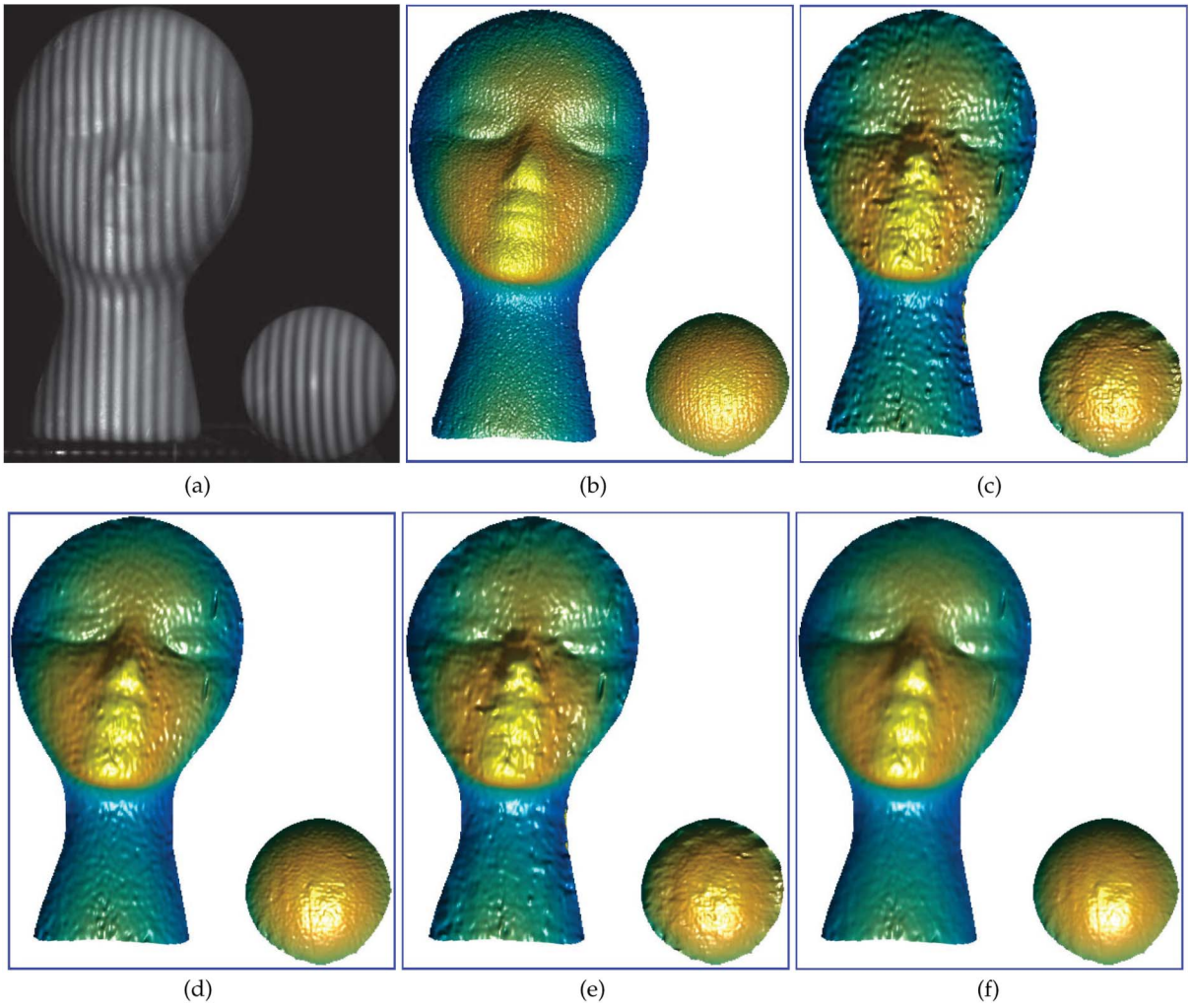

Fig. 9. 3D measurement results of two objects. (a) Captured fringe image; (b) using standard phase-shifting method plus simple binary coding; (c) using single-shot FTP method with smoothed circular-shaped bandpass filter; (d) using modified FTP method with smoothed circular-shaped bandpass filter; (e) and (f) corresponding results of (c) and (d) using a Hanning-window-shaped bandpass filter.

depth range with a given hardware setup through a software approach.

• *Inherent FTP limitations*. Our proposed framework does not contribute to improving the phase quality of FTP itself, and thus some common problems for the FTP approach remain in our proposed technique. For example, complex surface geometry variations and rich surface texture deteriorate phase quality and thus reduce measurement accuracy since the carrier phase cannot be accurately retrieved. However, those methods developed to improve the phase quality of FTP can also be adopted to improve measurement quality of the proposed method. As demonstrated in our paper, the modified FTP method using two fringe patterns can substantially improve measurement quality. One can also adopt the windowed Fourier transform (WFT) method [26,27] to improve the robustness of FTP to noise and enhance phase quality.

Even with these limitations, the pixel-by-pixel absolute 3D shape measurement capability enabled by the proposed method could substantially expand the applications of FTP where absolute 3D geometry measurement is required or multiple unknown object measurement is necessary.

5. CONCLUSION

In this research, we developed a computational framework that only requires one single grayscale fringe pattern for absolute 3D shape reconstruction. This framework performs phase unwrapping by pixel-to-pixel reference to the minimum phase map that is generated at the closest depth plane of the measured volume. Because our framework does not involve any additional encodings or embedded markers, it overcomes the current phase-unwrapping limitation of the single-shot FTP method. Our experiments have demonstrated the success of our proposed framework by measuring both single object and spatially isolated objects.

Funding. National Science Foundation (NSF) Directorate for Engineering (ENG) (CMMI-1531048).

Acknowledgment. We would like to thank other students in our lab, in particular, Ziping Liu and Chufan Jiang, for their assistance in hardware setup and experiments.

REFERENCES

1. D. Malacara, ed., *Optical Shop Testing*, 3rd ed. (Wiley, 2007).
2. Y. Wang, S. Zhang, and J. H. Oliver, "3D shape measurement technique for multiple rapidly moving objects," Opt. Express **19**, 5149–5155 (2011).
3. M. Takeda and K. Mutoh, "Fourier transform profilometry for the automatic measurement of 3-D object shapes," Appl. Opt. **22**, 3977–3982 (1983).
4. M. Takeda, "Fourier fringe analysis and its applications to metrology of extreme physical phenomena: a review," Appl. Opt. **52**, 20–29 (2013).
5. X. Su and Q. Zhang, "Dynamic 3-D shape measurement method: a review," Opt. Lasers Eng. **48**, 191–204 (2010).
6. S. Petitgrand, R. Yahiaoui, K. Danaie, A. Bosseboeuf, and J. Gilles, "3D measurement of micromechanical devices vibration mode shapes with a stroboscopic interferometric microscope," Opt. Lasers Eng. **36**, 77–101 (2001).
7. M. B. Whitworth and J. M. Huntley, "Dynamic stress analysis by high-resolution reflection moiré photography," Opt. Eng. **33**, 924–931 (1994).
8. H. Guo and P. S. Huang, "Absolute phase technique for the Fourier transform method," Opt. Eng. **48**, 043609 (2009).
9. Q. Hu, P. S. Huang, Q. Fu, and F.-P. Chiang, "Calibration of a three-dimensional shape measurement system," Opt. Eng. **42**, 487–493 (2003).
10. S. Zhang and P. S. Huang, "Novel method for structured light system calibration," Opt. Eng. **45**, 083601 (2006).
11. Y.-Y. Cheng and J. C. Wyant, "Two-wavelength phase shifting interferometry," Appl. Opt. **23**, 4539–4543 (1984).
12. Y.-Y. Cheng and J. C. Wyant, "Multiple-wavelength phase shifting interferometry," Appl. Opt. **24**, 804–807 (1985).
13. D. P. Towers, J. D. C. Jones, and C. E. Towers, "Optimum frequency selection in multi-frequency interferometry," Opt. Lett. **28**, 887–889 (2003).
14. J. Pan, P. S. Huang, and F.-P. Chiang, "Color-coded binary fringe projection technique for 3-D shape measurement," Opt. Eng. **44**, 023606 (2005).
15. Y. Wang and S. Zhang, "Novel phase coding method for absolute phase retrieval," Opt. Lett. **37**, 2067–2069 (2012).
16. S. Zhang and P. S. Huang, "High-resolution real-time three-dimensional shape measurement," Opt. Eng. **45**, 123601 (2006).
17. W.-H. Su, "Projected fringe profilometry using the area-encoded algorithm for spatially isolated and dynamic objects," Opt. Express **16**, 2590–2596 (2008).
18. S. Gai and F. Da, "A novel phase-shifting method based on strip marker," Opt. Lasers Eng. **48**, 205–211 (2010).
19. H. Cui, W. Liao, N. Dai, and X. Cheng, "A flexible phase-shifting method with absolute phase marker retrieval," Measurement **45**, 101–108 (2012).
20. B. Budianto, P. Lun, and T.-C. Hsung, "Marker encoded fringe projection profilometry for efficient 3D model acquisition," Appl. Opt. **53**, 7442–7453 (2014).
21. Y. Xiao, X. Su, Q. Zhang, and Z. Li, "3-D profilometry for the impact process with marked fringes tracking," Opto-Electron. Eng. **34**, 46–52 (2007).
22. J.-F. Lin and X. Su, "Two-dimensional Fourier transform profilometry for the automatic measurement of three-dimensional object shapes," Opt. Eng. **34**, 3297–3302 (1995).
23. L. Guo, X. Su, and J. Li, "Improved Fourier transform profilometry for the automatic measurement of 3D object shapes," Opt. Eng. **29**, 1439–1444 (1990).
24. B. Li, N. Karpinsky, and S. Zhang, "Novel calibration method for structured light system with an out-of-focus projector," Appl. Opt. **53**, 3415–3426 (2014).
25. S. Zhang, "Flexible 3D shape measurement using projector defocusing: extended measurement range," Opt. Lett. **35**, 931–933 (2010).
26. Q. Kemao, "Windowed Fourier transform for fringe pattern analysis," Appl. Opt. **43**, 2695–2702 (2004).
27. Q. Kemao, "Two-dimensional windowed Fourier transform for fringe pattern analysis: principles, applications and implementations," Opt. Lasers Eng. **45**, 304–317 (2007).